ACTA SCIENTIFIC APPLIED PHYSICS

Volume 1 Issue 1 December 2019

Research Article

New 3D and 2D Octa Carbon C_8 and Isoelectronic B_4N_4 Having Peculiar Mechanical and Magnetic Properties, from First Principles

Samir F Matar[1,2]*

[1]*Lebanese German University. Sahel-Alma, Jounieh, Lebanon*

[2]*Formerly at the University of Bordeaux, ICMCB–CNRS, Pessac, France*

***Corresponding Author:** Samir F Matar, **E-mail:** s.matar@lgu.edu.lb

Received: November 29, 2019; **Published:** December 08, 2019

Abstract

Cohesive energies, energy-volume equations of states EOS, electron localization ELF maps, elastic constants, and band structures are reported based on DFT calculations for original octacarbon C_8 three dimensional 3D and two-dimensional 2D chemical systems based on density functional theory calculations. Specifically, tetragonal C_8 is identified cohesive with hardness close to experimentally identified cubic Ia-3 C_8; both exhibiting comparable hardness to diamond. Also, isoelectronic and isostructural B_4N_4 is calculated with a slightly lower hardness due to the ionocovalent B-N bonding. 2D-C_8 ($C1_2C2_6$) on the other side is proposed with interpenetrating two carbon hexagonal substructures, C1 and C2, identified from energy calculations in a ferromagnetic ground state; this constitutes an original result in so far that p-magnetism is unusual. Electronic band structures analysis identifies insulating behaviors for 3D C_8 and B_4N_4 while 2D-C_8 ($C1_2C2_6$) is characterized by different bands for magnetic carbon substructure (C1) from non-magnetic semi-conducting honeycomb-like $C2_6$ layers. These latter observations let propose spin chemistry perspectives once such multilayered carbon 2D compounds are grown as stand-alone or on selected substrates as thin or thick films.

Keywords: DFT; Hard and Soft Materials; Dimensionality; Magnetism

Introduction

Life and nature are based on carbon as the major constituent. But as such, carbon atoms organization into lattices and structures offer a broad range of possibilities regarding dimensionality factor that we focus upon in this work. Besides fullerene C_{60}, zero-dimensional 0D carbon can be formed into 'dots' entering biosciences applications such as by stabilizing insulin [1]. 1D carbon is mainly illustrated by carbon nanotubes; cf. review by Sinnott., *et al*. on its syntheses and applications; some of them pertaining to dimensional and chemical compatibility issues with biomolecules (DNA, proteins, ...) [2]. Much earlier than technologically elaborated carbon, naturally occurring graphite (2D) and diamond (3D) were known and intensively used. The transformation of graphite into diamond occurs into Earth D'' mantle near volcanoes and tectonic plates, i.e. where the necessary high pressures P >150 kbar and temperatures T ~1200°C are found. However, the transformation kinetics is very slow and several millennia are required for obtaining a natural diamond. Mimicking Earth P, T conditions, the manmade artificial diamond was fabricated in the laboratory and 'General Electric' company was the first to produce it in the 1950s [3,4]. Nevertheless, besides its high cost, industrial applications of artificial diamond grafted on tooling machines are hindered by its instability at elevated temperatures generated by the friction involved in the process. Rapidly other substitutes to diamond were sought and boron nitride BN is a manmade binary which is isoelectronic of carbon. Indeed 2C ≡ B + N, i.e. 2 C($2s^2$,$2p^2$) ≡ B($2s^2$,$2p^1$) + N($2s^2$,$2p^3$) summing up to 8 electrons on each side of equivalence sign ≡. Boron nitride takes overall carbon forms, even nanotubes. In the context of present works, it is relevant to point out that BN nanotubes were theoretically devised prior to fabrication by Rubio ate al. back in 1994 [5]. BN can be synthesized in both 2D *h*-BN (white graphite, used as a lubricant) and 3D forms. Cubic boron nitride *c*-BN has a hardness close to that of diamond [3]; it usefully substitutes to it in tooling machines, due to its better resistance to elevated temperatures with its refractory properties characterized by a high melting temperature of T_{melt}~3000°C. Also within the BCN ternary diagram several other artificially devised 2D and 3D new materials were identified by combined experimental and modeling approaches leading to predict new compounds with well-targeted properties as extreme hardness (cf. ref. [6] for an overview). For instance β-C_3N_4 was predicted by Liu and Cohen with a larger hardness than that of diamond [7] and in 2001 BC_2N was predicted with larger hardness than *c*-BN [8] simultaneously with and independently from its synthesis by Vladimir Solozhenko research group in Villetaneuse-Paris [9]. Clearly, this research field has benefited from theoretical predictions helping subsequent syntheses thanks to the accuracy of quantum-physics based calculations within the density functional theory (DFT) [10,11].

Back to carbon, in 1989, octacarbon C_8 [12] was announced as denser than diamond whose structure is given in Figure 1a while C_8 is shown in Figure 1b; the crystal data are given in Table 1. Both structures feature the characteristic distances which are all close to 1.5 Å. More recently DFT calculations let predict octa-silicon Si_8 new allotrope with potential applications to Li-battery anode materials [13].

Following this long contextual introduction, the present paper aims at highlighting the dimension (3D and 2D) – electronic (and mechanical properties) relationship effects of C_8 octacarbon. Also, in the above context of isoelectronic $2C \equiv B + N$ leading to similarly behaving binary (BN) versus unary (C) compounds, original tetraboron nitride B_4N_4 with a 3D tetragonal structure is proposed as a hard material (cf. Figure 1d). The original properties result from dimensionality, i.e. respectively ultra-hard 3D C_8 and B_4N_4 and ultra-soft layered 2D C_8. Specifically, the latter expressed as $C1_2C2_6$ is formed of interpenetrating two carbon substructures one of them (C1) undergoing magneto-volume effects oppositely to nonmagnetic host C2 hexa-layers (cf. Figure 1e). Also, 2D-C8 is found to possess a long-range ferromagnetic order for one of the two carbon substructures.

(a)

(b)

(c)

(d)

(e)

Figure 1: Crystal structures of the carbon systems (and B_4N_4) under consideration: a) Diamond; b) C_8 Ia-3 ; c) C_8 P4/mmm ; d) B_4N_4 P4/mmm; e) Magnetic 2D-C_8 P6/mmm. Remarkable distances in Å are shown. Drawings were produced by VESTA ref. K. Momma and F. Izumi, "VESTA 3 for three-dimensional visualization of crystal, volumetric and morphology data", J. Appl. Crystallogr., 44, 1272-1276 (2011).

Computational framework

For the sake of fully defining the ground structure, geometry optimizations of the atomic positions and lattice parameters were carried out to minimize the inter-atomic forces using plane-wave VASP code [14,15]. Within DFT, VASP is based on the projector augmented wave (PAW) method [15, 16]. The generalized gradient approximation (GGA) accounting for DFT effects of exchange and correlation was used [17]. The atoms were relaxed into the ground state with the help of a conjugate-gradient algorithm [18]. Structural parameters were considered to be fully relaxed when forces on the atoms were less than 0.02 eV/Å^3 and all stress components below 0.003 eV/Å^3. An energy cut-off of 500 eV for the plane-wave basis set was used and the tetrahedron method was applied according to Blöchl [19] for both geometry relaxation and total energy calculations. Brillouin-zone (BZ) integrals were approximated using the special k-point sampling of Monkhorst and Pack [20] and successive calculations with increasing precision of BZ integration were carried to reach the highest accuracy.

A major outcome of the calculations is the rationalization of the electron localization, thus addressing the question: "where are the electrons"? which can be achieved thanks to the electron localization function (ELF) mapping. ELF introduced by Becke and Edgecomb [21] initially for Hartree–Fock calculations was extended later on to DFT methods by Savin., *et al*. [22]. Based on the kinetic energy in which the Pauli Exclusion Principle is included: ELF = $(1+\chi_\sigma^{2})^{-1}$ with $0 \leq \text{ELF} \leq 1$, is a normalized function. In this expression the ratio $\chi_\sigma = D_\sigma/D_\sigma^{0}$, where $D_\sigma = \tau_\sigma - \frac{1}{4}(\nabla\rho_\sigma)^2/\rho_\sigma$ and $D_\sigma^{\circ} = 3/5\,(6^2)^{2/3}\,\rho_\sigma^{5/3}$ correspond respectively to a measure of Pauli repulsion (D_σ) of the actual system and to the free electron gas repulsion (D_σ^{0}) and τ_σ is the kinetic energy density. The normalization of the function is between 0 (zero localization) and 1 (strong localization) with the value of ½ corresponding to a free electron gas scheme. The maps are then analyzed following color code such that blue zones correspond to zero localization, red zones correspond to full localization and green zones with ELF= ½. Besides the 2D ELF representation, we consider the corresponding 3D isosurfaces relevant to define localization domains of coordination as tetrahedral and hexagonal (cf. Figure 2).

(a)

(c)

(b)

(d)

Figure 2: Electron localization 3D and 2D mapping over multiple adjacent cells in 3D tetragonal C_8 (a), in 3D B_4N_4 (b) and 2D C_8 ($C1_2C2_6$). See text for assessments and color codes.

Calculations and Results

Geometry optimization

3D-phases (C_8 and B_4N_4)

Based on octa-silicon Si_8 [13] and replacing Si by C in a primitive cell, C_8 was calculated in the P4/mmm space group (N°123). The structural data resulting from full unconstrained energy calculations with VASP are provided in Table 1a. The C-C distance of 1.51 Å is smaller than in diamond and body-centered cubic C_8 (cf. Figure 1b). In the simple tetragonal space group, the carbon atoms are dispatched into two substructures as depicted in Figure 1c. The structure is close to the one found for plasma deposited octacarbon by Natyushenko., *et al*. back in 1981 [23].

Based on these results obtained for C_8 and using the isoelectronic rule between 2C and BN, B_4N_4 was calculated along with two hypotheses: Hypothesis 1: B and N occupy the two carbon substructures of C_8; hypothesis 2: B and N are redistributed within the same plane.

Hypothesis 1 leads to the presence of B-B, N-N unphysical connections besides B-N realistic bonds, whereas hypothesis 2 offers a chemical setup with B-N connections, prevailing over the structural weakness of B-B and N-N nearest neighbors. This was also found with a much better cohesive energy. The structure with hypothesis 2 was then submitted to unconstrained geometry optimization. The resulting calculated data are provided in (Table 1b) and the structure is displayed in Figure 1d. The higher *a* parameter is due to the larger atomic size of B (r_B= 0.82 Å) and the fact that the average (r_B + r_N)/2 =0.785 > r_C = 0.770. The effects of the chemical bonding change from purely covalent (C-C) to iono-covalent due to the coexistence of two chemically different species B and N- are noticeable they will be quantitatively and illustrated with the ELF maps (cf. Figure 2) in next sections.

2D-C8 phase

Regarding 2D carbon-based layer compounds, we recently identified from ab initio the occurrence of magnetic instabilities on nitrogen in carbon-rich nitrides as C_6N [24]. The structure belongs to the P6/mmm space group (N°191) in a sort of extended AlB_2-type hexagonal structure. Such a layered structure is based on experimental evidence of Li-C electrodes for batteries [25]. The 2D-C8 proposed originally here has a structure shown in Figure 1d). It consists of two interpenetrating carbon substructures C1 and C2 with 2 C1 at 2.42 Å separation sandwiched between 6 C2 forming a honeycomb network with d(C2–C2) = 1.40 Å. Calculations were carried out in both non-spin-polarized (NSP) nonmagnetic and spin-polarized (SP) magnetic configurations in so far that similar trends of the onset of finite magnetizations were identified in extended carbonitride systems [24].

The results of full geometry relaxations into the minimum energy ground state are shown in Table 1c. While *a* lattice constant remains almost the same in both NSP and SP the configurations leading to similar magnitudes of interatomic distance above, there is a large increase of *c/a* hexagonal ratio from 1.55 to 1.67 pointing to a larger volume upon the onset of magnetization which amounts to 1.8 μ_B. The increase of the c/a hexagonal parameter and not the "*a*" parameter likely arises from the rigidity of the structure involved with the planar carbon honeycomb network in the plane shown in Figure 1d. Also the structure of the magnetically polarized C_8 is differentiated from the non-magnetic one by the increase of the c/a ratio. The SP total energy is lower than the NSP one. Then it can be proposed that the ground state of 2D-C8 is ferromagnetic. This was further confirmed from antiferromagnetic calculations assigning opposite spins to the two C1 atoms as well as making half the C2 constituents as SPIN UP and the other half SPIN DOWN. The calculations led to a decrease of magnetic moments and a raise of energy by 0.8 eV, leading to confirm the ferromagnetic ground state.

Cohesive energies

The difference between total electronic energies and the sum of the constituents' energies allows obtaining the cohesive energies. These are needed to validate further the geometry optimized structures and establishing trends between related compounds. Table 2 gathers the results for the energies of different atomic constituents and compounds under consideration. The trends can be established upon averaging the cohesive energies as per atomic constituent: $E_{coh.}$/at.

Space group	**C_8 Ia-3 [4]**	**C_8 P4/mmm (*)**
a	4.29 (4.47)	4.38
c/a		0.57
Atomic positions		
C1	(16c) 0.104 (0,094), x,x	(4j) 0.180,0.180,0
C2		(4k) 0.321,0.321, ½
d(C1-C1)	1.54 (1.52)	1.51

a) 3D C_8 phases.

	B_4N_4
a	4.40
c/a	0.58
Atomic positions	
B	0.174, x, 0 0.826, x, 0 0.675, 1-x, ½ 0.325, 1-x, ½
N	0.813, 1-x, 0 0.187, 1-x, 0 0.313, x, ½ 0.675, x, ½
d(B-N)	1.53
d(B-B)	1.77
d(N-N)	1.61

b) 3D B4N4 phase tetragonal P4/mmm space group.

P6/mmm	NSP	SP
a	4.18	4.19
c/a	1.55	1.67
Total energy (eV)	-61.37	-61.48
Volume	97.83	111.57
C1	(2d) 1/3, 2/3, ½	(2d) 1/3, 2/3, ½
C2	(6j) 0,0.333,0	(6j) 0,0.333,0
d(C1-C1)	2.42	2.42
d(C2-C2)	1.39	1.40
M (μ_B)	-	1.80

c) 2D C8.

Table 1: C_8 and B_4N_4 new forms in 3D and 2D dimensional structures. Experimental and (calculated) data for C_8 Ia-3 and calculated parameters for other original compounds. The lattice parameters and the interatomic distances are expressed in Å unit.

Citation: Samir F Matar. "New 3D and 2D Octa Carbon C_8 and Isoelectronic B_4N_4 Having Peculiar Mechanical and Magnetic Properties, from First Principles". *Acta Scientific Applied Physics* 1.1 (2019): 15-22.

Compound	**S.G.**	**$E_{Tot.}$/8FU**	**$E_{coh.}$/at.**
Diamond	F-43m	–72.76	–1.985
3D-C_8	Ia-3	–67.14	–1.283
3D-C_8	P4/mmm	–71.18	–1.786
3D-B_4N_4	P4/mmm	–57.69	–1.019
2D- C_8	P6/mmm	–61.47	–0.574

Table 2: Diamond, octacarbon and B_4N_4 forms. Trends of cohesive energies (E_V). Energy per constituent atom: E(C) = –7.11 eV; E(B)= –5.55 eV; E(N)= –6.82 eV. S.G: Space group.

Diamond is most cohesive while 2D- C_8 is the least cohesive; the other 3D compounds being found in between. Note that the newly proposed tetragonal C_8 is more cohesive than body-centered cubic C_8 (*Ia*-3) and its cohesive energy is closer to that of Diamond. B_4N_4 shows much lower cohesive energy than the pure carbon 3D phases proposed in spite of the isoelectronic character of B_4N_4 and C_8. This arises from the different chemical natures of B and N versus C, i.e. the difference between C-C and B-N bonding. Such a feature can be further supported upon visualizing the electron localization in these chemical systems through the Electron Localization Function (ELF).

Electron localization function visualization

The ELF 3D isosurface and 2D maps are shown in Figure 2 projected over multiples cells for the sake of clear presentation. Relevant to the above discussion are the representations of 3D tetragonal C_8 and isoelectronic B_4N_4 where 3D isosurfaces and 2D slices along vertical diagonal plane are shown to highlight the covalent C-C versus the B-N ionocovalent bonds. Indeed there is an opposite behavior whereby there is a centered torus-like halfway between two carbons in C_8 signaling a perfectly covalent bond (as in diamond) whereas the grey isosurface has a half-moon shape in B_4N_4 pointing to nitrogen signaling an iono-covalent bond polarized away from electropositive boron. Also, the tetrahedral coordination can be clearly seen. The opposite natures of the bonds are further illustrated on the right-hand side panels with 2D slices with high localization red areas surrounding the 3D isosurface with a clear differentiation between B surrounded with free-electron like green areas oppositely to nitrogen surrounded with red strong localization ELF. It will be shown in the next sections that the major impact of such chemical properties will be on the respective hardness of C_8 versus B_4N_4.

Turning to P6/mmm hexagonal C_8, the 2D and 3D ELFs around C1 are different from the honeycomb C2 ELFs especially for the half-moon like 3D grey surface on each side signaling non-bonded electrons which eventually polarized magnetically; the feature of off-plane electron localization is shown with a slice at z~0.4 which exhibits red areas signaling strong localization. In spite of the 2.4 Å separation there is significant electron localization of free electron like nature (green ELF ~ ½) showing a non-negligible chemical interaction between the 2 C1 via σ electrons while the out-of-plane electrons are relevant to π-like; the whole ensemble of valence 2s and 2p C electrons being hybridized in molecular nomenclature as sp^2. Looking at the slice crossing the C2 substructure, the bonding between adjacent C2 atoms is different from the red localization areas between adjacent C2 atoms. So the two carbon substructures are quite different in electronic and bonding characters.

Energy-volume equations of states and structural stability

In order to fully establish the ground state (magnetic) structure, the energy-volume equations of state (EOS) are required. The EOS used here is Birch's [26] expressed up to the 3rd order as:

$$E(V)= E_o(V_o)+[9/8]V_oB_o[([(V_o)/V])^{[2/3]}-1]^2+[9/16]B_o(B'-4)V_o[([(V_o)/V])^{[2/3]}-1]^3,$$

where E_o, V_o, B_o and B' are the equilibrium energy, the volume, the bulk modulus, and its pressure derivative.

In both cases calculated B'= 3.6. The fits are done over (E, V) sets of calculations around minima found from the geometry optimization. Figure 3 shows the E,V curves and the fit values in the inserts for the different compounds. Focusing on the B_0 magnitudes of the 3D compounds, there is a regular decrease from diamond (B_0= 420 GPa) down to B_4N_4 (B_0= 350 GPa). B_4N_4 is found slightly more compressible than cubic BN with B_0 ~396 GPa, [24] but remains a good ultra-hard material candidate, especially with regard to its calculated cohesive energy. Tetragonal C_8 is found highly incompressible with hardness close to that of super-dense body-centered C_8 (B_0=416 GPa). Clearly, the argued upon covalent versus iono-covalent characters discussed above and illustrated with the ELF can underlie these results.

Then for 2D-C8 expressed as $C1_2C2_6$, both NSP and SP EOSs were established. The E,V curves are shown in Figure 4. The SP curve versus the NSP one is at lower energy and larger volume due to the development of magnetization. It can be observed also that the larger the volume (SP) the lower the bulk module is. The rather small difference of volume ΔV(SP-NSP) = 8 $Å^3$ is accompanied by ΔE(SP-NSP) = -0.15 eV and let suggest that the passage from SP to NSP configuration can be induced by external effects as pressure. The P magnitude can be estimated from the Birch relationship providing the pressure [26]:

$$P_C = (B_o/B')\ [(V_o/V')^{B'}-1]$$

where B_0 and V_0 correspond to the SP configuration from which one departs to compress the system and V_1 the NSP volume. Then one calculates P_C = 12 GPa. This magnitude is much smaller than that required for vanishing magnetization for ferromagnetic oxides as CrO_2 (P_C = 150 GPa) as well as intermetallic alloys systems as Fe-Ni (P_C = 55 GPa) [27]. The 2D-C_8 can be assigned "soft" magnetic behavior while CrO_2 is a "hard" ferromagnet [28].

Citation: Samir F Matar. "New 3D and 2D Octa Carbon C_8 and Isoelectronic B_4N_4 Having Peculiar Mechanical and Magnetic Properties, from First Principles". *Acta Scientific Applied Physics* 1.1 (2019): 15-22.

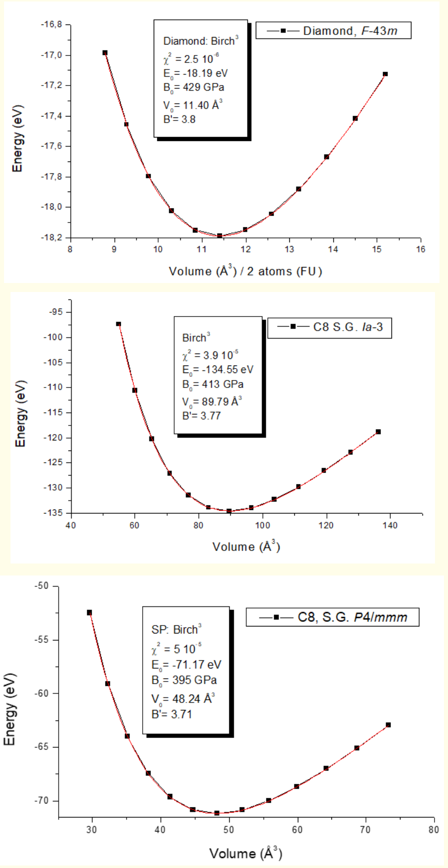

Figure 3: 3D carbon derived compounds: cubic diamond, body-centered C_8 and new 3D carbon C_8 and tetragonal boron nitride B_4N_4 phases: Energy - volume quadratic curves and fit parameters (inserts) of 3rd order equation of states (EOS) (see text).

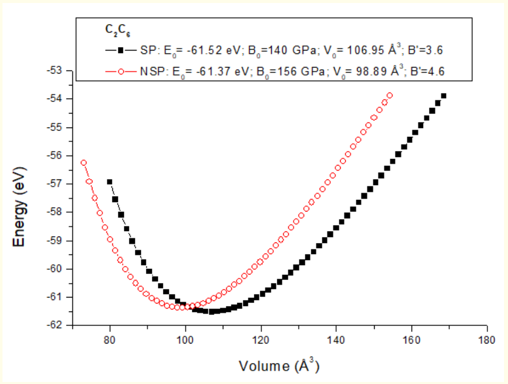

Figure 4: 2D octacarbon phase C_2C_6: Energy-volume quadratic curves and fit parameters (inserts) of 3rd order EOS.

Structural stability

Stressing further the results, the structural stability was established based on deriving the elastic constants. The elastic properties are determined by performing finite distortions of the lattice and deriving the elastic constants from the strain-stress relationship. In tetragonal and hexagonal symmetries there are six independent elastic stiffness constants C_{11} C_{12} C_{13} C_{33} C_{44} C_{66}. The most widely used method of evaluating the elastic stiffness constants is the method of Voigt [26] based on a uniform strain. For the purpose of establishing structural stability of newly proposed 3D and 2D C_8 calculations of the respective elastic constants were carried out. The obtained values are given in units of GPa (gigaPascal pressure):

3D-C8 P4/mmm: $C_{11}= C_{22}=930$; $C_{12}=170$; $C_{13}=57$; $C_{33}=1186$; $C_{44}=321$; $C_{66}=446$

3D-B_4N_4 P4/mmm: $C_{11}= C_{22}=725$; $C_{12}=167$; $C_{13}=105$; $C_{33}=955$; $C_{44}=241$; $C_{66}=328$

and 2D-C8 P6/mmm: $C_{11}= C_{22}=477$; $C_{12}=117$; $C_{13}=25$; $C_{33}=200$; $C_{44}= 180$; $C_{66}=13$.

As a general trend, all C_{ij} magnitudes are much larger in 3D versus 2D, thus translating the high softness of the latter. All three compounds are structurally stable is so far that the C_{ij} magnitudes are positive while complying with the stability rules pertaining to the mechanical stability:

$$C_{11} > C_{12};\ C_{11}C_{33} > C^2_{13};\ (C_{11} + C_{12})C_{33} > 2\ C^2_{13}$$

Quantitatively these C_{ij} magnitudes are rationalized by the calculation of the bulk modulus labeled B_V following Voigt [29]:

$$B_V = 1/9\ \{2(C_{11} + C_{12}) + 4C_{13} + C_{33}\}$$

Numerically:

$B_V = 400$ GPa for 3D-C_8, $B_V = 340$ GPa for 3D-B_4N_4 and $B_V= 159$ GPa for 2D-C8.

These bulk module magnitudes arising from the calculated elastic constants come close to the values obtained from the EOS fit of the E,V curves. This validates the two approaches and confirms the trends announced.

Electronic band structure calculations

The electronic band structures of the different compounds were calculated in the respective Brillouin Zones at high ***k***- mesh integration. Figure 5 shows in 4 panels the band structures of the 3D compounds. The zero-energy along the *y*-axis is with respect to the top of the (occupied) valence band VB (E_V) separated from the (empty) conduction band CB by an energy gap, leading to the ($E-E_V$) eV labeling. The *x*-axis spans the main directions of the irreducible respective BZ's.

Figure 5: Electronic band structures of three dimensional (3D) title compounds.

Starting with diamond the bandgap is ~5 eV as commonly found in the literature (cf. [30] and therein cited works). With body-centered cubic $C_{8,}$ the bandgap decreases to half its magnitude while in tetragonal C_8 the gap magnitude increases again up to ~4 eV. The widest VB is observed for B_4N_4 and the separation from CB is very large with the bandgap ~5 eV almost the same as in diamond. This is an interesting result, knowing the large chemical differences between C and BN. The bands have the same shape as tetragonal C_8 in spite of the small distortion of the lattice due to the atomic rearrangement and the symmetry decrease due to the loss of the 4-fold (C_4) vertical symmetry axis and its replacement by a 2-fold (C_2) symmetry axis.

Regarding 2D-C_8, Figure 6 shows the band structures differentiated for the non-magnetic substructure C2 (top) and magnetic C1 (bottom) for the sake of clarity. For the C2 substructure comprising six atoms forming a honeycomb network (Figure 1 and 2), there is a small bandgap as in graphite and the energy reference is with respect to E_V top of the VB. This is opposed to C1 substructure which shows two sets of bands separated by small energy magnitude due to the magnetic polarization whereas C1 bands show splitting into majority spin bands (↑) at lower energy than higher energy bands corresponding to minority spins (↓). The energy split between the two spin populations involves all bands even the low energy s bands. This can be assessed within a molecular like scheme whereby there is hybridization (quantum mixing) of s and p valence state of carbon provide sp^2-like planar hybridization with one σ electrons connecting the two C1 carbon atoms and (cf. Figure 2c) and off-plane 2π like. Oppositely to C2 substructure, there is no gap between VB and CB and C1 bands cross the top of VB at E_F (Fermi energy) because of the metallic character characterizing C1 substructure. The corresponding population difference (↑ - ↓) provides the magnetization which amounts to 0.9 μ_B1specifically at C1 site. Clearly, we are presented with two interpenetrating carbon substructures behaving differently while being in the same 2D structure C_8.

Synthesis efforts using pulsed laser deposition (PLD) or chemical vapor deposition (CVD) are underway in collaboration with the

Figure 6: Electronic band structures of 2D C_8 ($C1_2C2_6$) in magnetic configuration, highlighting semi-conducting behavior within $C2_6$ substructure and spin polarization within $C1_2$ bands with a total magnetization of 1.8 μ_B.

Bibliography

1. Xu Han., *et al*. “Interactions between Carbon Nanomaterials and Biomolecules”. *Journal of Oleo Science* 65 (2016) 1-7.
2. B Sinnott and R Andreys. “Carbon Nanotubes: Synthesis, Properties, and Applications”. *Critical Reviews in Solid State and Materials Sciences* 26 (2001): 145-249.
3. G Demazeau. “High pressure in solid-state chemistry”. *Journal of Physics: Condensed Matter* 14 (2002): 11031.
4. RM Hazen. “The Diamond Makers”. Cambridge U. P., New York (1999).
5. A Rubio., *et al*. Theory of graphitic boron nitride nanotubes”. *Physical Review B* 49 (1994): 5081.
6. J Etourneau and SF Matar. *Solid State Sciences* 80 (2018) 178.
7. A Liu and ML Cohen. “Prediction of new low compressibility solids”. *Science* 245 (1989): 841.
8. M Mattesini and SF Matar. “First-principles characterisation of new ternary heterodiamond BC2N phases”. *Computational Materials Science* 20 (2001): 107.
9. VL Solozhenko., *et al*. “2.5% efficient organic plastic solar cell”. *Applied Physics Letters* 78 (2001): 1385.
10. P Hohenberg and W Kohn. “Inhomogeneous Electron Gas”. *Physical Review B* 136 (1964): 864.
11. W Kohn and LJ Sham. “Self-Consistent Equations Including Exchange and Correlation Effects”. *Physical Review A* 140 (1965): 1133.
12. RL Johnston and RJ Hoffmann. “Superdense carbon, C8: supercubane or analog of .gamma.-silicon?”. 111 (1989): 810.
13. Wu Fang., *et al*. “Density functional predictions of new silicon allotropes: Electronic properties and potential applications to Li-battery anode materials”. *Solid State Communications* 151 (2011): 1228.
14. G Kresse and J. Furthmüller. “Efficient iterative schemes for ab initio total-energy calculations using a plane-wave basis set”. *Physical Review B* 54 (1996): 11169.
15. G Kresse and J Joubert. “From ultrasoft pseudopotentials to the projector augmented-wave method”. *Physical Review B* 59 (1999): 1758.
16. PE Blöchl. “Projector augmented-wave method”. *Physical Review B* 50 (1994): 17953.
17. J Perdew., *et al*. “Generalized Gradient Approximation Made Simple”. *Physical Review Letter* 77 (1996) 3865.
18. WH Press., *et al*. Numerical Recipes, New York: Cambridge University Press (1986).
19. P.E. Blöchl., *et al*. “Improved tetrahedron method for Brillouin-zone integrations”. *Physical Review B* 49 (1994): 16223.
20. HJ Monkhorst and JD Pack. “Special points for Brillouin-zone integrations”. *Physical Review B* 13 (1976): 5188.
21. D Becke and KE Edgecombe. “A simple measure of electron localization in atomic and molecular systems”. *The Journal of Chemical Physics* 92 (1990): 5397.
22. A Savin., *et al*. “Electron Localization in Solid-State Structures of the Elements: the Diamond Structure†”. 31 (1992): 187.
23. NN Natyushenko., *et al*. Soviet Physics, Crystallography 26 (1981): 274.
24. SF Matar. *Journal of Magnetism and Magnetic Materials* 469 (2019): 46.
25. Dolotko., *et al*. *Journal of Power Sources* 255 (2014): 197.
26. F Birch. “Finite strain isotherm and velocities for single-crystal and polycrystalline NaCl at high pressures and 300°K”. *Journal of Geophysics Research* 83 (1978): 1257.
27. P Mohn., *et al*. “Calculated electronic and magnetic structure of the nitrides NiFe3N and PdFe3N”. *Physical Review B* 45 (1992): 4000.
28. SF Matar and G Demazeau. *Chemical Physics Letters* 407 (2005): 516-521.
29. W Voigt. “Lehrbuch der Kristallphysik”. Vieweg + Teubner, Wiesbaden (1966).
30. M Mattesini and SF Matar. *International Journal of Inorganic Materials* 3 (2001): 943-957.

Volume 1 Issue 1 December 2019

Citation: Samir F Matar. “New 3D and 2D Octa Carbon C_8 and Isoelectronic B_4N_4 Having Peculiar Mechanical and Magnetic Properties, from First Principles". *Acta Scientific Applied Physics* 1.1 (2019): 15-22.